NUMERICAL SIMULATION OF DROPLET EVAPORATION BASED ON THE SMOOTHED PARTICLE HYDRODYNAMICS METHOD

by

Xinpeng XIAO, Xiaojing MA*, Tusongjiang KARI, Qiang XU, and Mengyao FAN

College of Electrical Engineering, Xinjiang University, Urumqi, China

Original scientific paper
https://doi.org/10.2298/TSCI230311101X

Based on the smoothed particle hydrodynamics method, a numerical model of smoothed particle hydrodynamics in multi-phase flow evaporation accompanied with heat and mass transfer has been established, and phase transition of droplet evaporation is simulated. In this paper, an smoothed particle hydrodynamics mass transfer equation of gas phase in evaporation are proposed based on Fick's law. In order to solve the problem of large mass difference of particles at the phase interface during evaporation, the particle splitting and merging techniques are introduced, and the tensile instability of particles during the splitting and merging is weakened by artificial stress. Besides, by adding the surface tension model, the mutual penetration of particles at the gas-liquid interface is effectively prevented. On this basis, the evaporation of single droplet and interacting droplets without gravity is simulated. The results show that the evaporation time of single droplet in this study conforms to D^2 law and is within the theoretical range. There is a great influence between interacting droplets in the process of evaporation. Only when dimensionless number C (droplet spacing/droplet diameter) is larger than eight, the influence between droplets can be approximately ignored.

Key words: *smoothed particle hydrodynamics, droplet evaporation, interacting droplets, surface tension, particle splitting and merging technique*

Introduction

Since Godsave [1] and Spalding [2] established the basic single droplet evaporation models and proposed the famous D^2 *law* in 1950's. Nomura *et al.* [3] experimentally investigated the droplet evaporation process in microgravity environment, focusing on the effects of temperature and pressure on the evaporation process, and the results showed that the droplet lifetime decreases with increasing external ambient temperature and is not correlated with ambient pressure when the temperature is higher than 480 K. The influence between interacting droplets in the process of evaporation is crucial. Labowsky [4], Sangiovanni and Labowsky [5], and Marberry *et al.* [6] studied extensively the interactions between the droplets in the case of monodisperse droplet streams. To describe the influence of the droplet interactions on the evaporation rate and the drag coefficient, they introduced the spacing parameter, C, which is defined as the ratio between the inter-droplet distance, L, and the droplet diameter, d. Castanet *et al.* [7] studied the heat and mass transfer characteristics of droplet and effect of droplet interactions on droplet evaporation in the case of monodisperse droplet streams.

* Corresponding author, e-mail: maxiaojing1983@xju.edu.cn

In addition, a large number of scholars used numerical methods to study the droplet evaporation problem. Chiang and Sirignano [8] were one of the first to investigate numerically the evaporation of interacting droplets moving relatively to the carrier gas by solving the Navier-Stokes equations. Tanguy *et al.* [9] proposed a numerical method using both the level-set method and the ghost fluid method to capture the interface motion and to handle conditions at the interface. Safari *et al.* [10, 11] proposed a lattice Boltzmann method to simulate the phase transition of multi-phase flow evaporation. Nikolopoulos *et al.* [12] investigated the evaporation process of *n*-heptane and water droplets impinging on a hot surface using the finite volume method coupled with the volume of fluid (VoF) method. Tonini *et al.* [13] developed a novel evaporation model for multi-component spherical drop by analytically solving the Stefan-Maxwell equations under spherical symmetry assumptions.

As a Lagrangian meshless particle method, smoothed particle hydrodynamics (SPH) method has the advantages of dealing with free surface, deformation boundary, moving interface and extreme deformation [14]. Monaghan *et al*. [15] used SPH method for the first time to conduct exploratory numerical simulation of solidification process. Zhang *et al*. [16] proposed a surface tension model and a latent heat model to solve the problem of heat exchange phase transition caused by droplet impact on cryogenic wall surface, and made a comparative analysis with relevant experimental results. Yang and Kong [17] proposed particle splitting and merging techniques to solve the problem of large mass difference problem of particles at the phase interface in the process of droplet evaporation and mass transfer. Drawing on the idea of VoF method Wang *et al*. [18] proposed the concept of liquid phase mass fraction of SPH particles to effectively characterize the phase transition process of evaporation. Li *et al*. [19] used the numerical method of smoothed particle hydrodynamics with adaptive spatial resolution (SPH-ASR) to study the effects of droplet diameter, impact velocity, liquid evaporation, wall temperature and the inclined angle of wall on droplet impact on hot wall.

In this paper, a 2-D numerical model of SPH in multi-phase flow evaporation with heat and mass transfer is established. Gas phase mass transfer equation is proposed in conjunction with Fick's law and the particle splitting and merging techniques are introduced to deal with the large mass difference between SPH particles, while artificial stress is adopted to weaken the stress changes during particle splitting and merging. The surface tension model is introduced and verified. On this basis, the single droplet evaporation is simulated, which is compared with the D^2 *law* and theoretical evaporation time. In order to explore the influence between droplets, interacting droplet evaporation is simulated.

The SPH-based numerical method for droplet evaporation

Governing equations

In SPH, eq. (1) is the integral expression of function, $f(x)$. In order to eliminate the inter-particle stretch instability, the smooth function is adopted:

$$f(x) \approx \int_{\Omega} f(x')W(x-x',h)\mathrm{d}x' \tag{1}$$

$$W(s,h) = \frac{1}{3\pi h^2}\begin{cases} s^3 - 6s + 6, & 0 \le s < 1 \\ (2-s)^3, & 1 \le s < 2 \\ 0, & 2 \le s \end{cases} \tag{2}$$

where $W(x - x', h)$ presents a smooth function and h is the stands for smoothing length. Where $s = r/h$, which r is the distance between particles.

The evaporation of droplet in the gas phase environment is coupled with large density difference at the phase interface and heat and mass transfer phenomena. Based on the conservation law, the equations of mass, momentum, energy and component conservation in Lagrangian form are listed:

$$\frac{\mathrm{d}\rho}{\mathrm{d}t} = -\rho\nabla u + \dot{m}''' \tag{3}$$

$$\frac{\mathrm{d}u}{\mathrm{d}t} = \mathrm{g} - \frac{1}{\rho}\nabla p + \frac{\mu}{\rho}\nabla^2 u + f_s \tag{4}$$

$$\frac{\mathrm{d}T}{\mathrm{d}t} = \frac{1}{\rho C_p}\nabla(k\nabla T) + \frac{h_v}{\rho C_p}\dot{m}''' \tag{5}$$

$$\frac{\mathrm{d}Y}{\mathrm{d}t} = \frac{\nabla(\rho D\nabla Y)}{\rho} \tag{6}$$

where ρ is the fluid density, u – the fluid velocity, p – the fluid pressure, g – the gravitational acceleration, μ – the dynamic viscosity, f_s – the surface tension, T – the temperature, C_p – the specific heat at constant pressure, k – the thermal conductivity, $\dot{m}'''$ – the volumetric mass evaporation rate, h_v – the latent heat of evaporation, Y – the vapor mass fraction, and D – the mass diffusivity of the vapor. Note that in this paper the production of thermal energy by viscous dissipation is not considered in the energy equations because of its relatively small magnitude [9, 10, 20]. The choice of time step Δt is determined by advection constraint $\Delta t \leq CFLh/c$. The c stands for a numerical speed of sound which is 10 times the flow field velocity, and $CFL = 0.2$. The governing aforementioned equations are not closed. This needs to adopt the volume-mass evaporation rate equation solve the mass transfer and the weakly compressible state equation solve the pressure term [17]:

$$\dot{m}''' = \frac{\dot{m}}{V} = \frac{\nabla(\rho D\nabla Y)}{1-Y} \tag{7}$$

$$p = c^2(\rho - \rho_r) + p_r \tag{8}$$

where $\dot{m}$ is the mass evaporation rate across the phase interface, V – the volume of particle, ρ_r – the reference density which is the initial density of the gas liquid phase, p_r – the reference pressure which is 150 Pa to prevent negative pressure.

For multi-phase flow, discontinuities in certain fluid properties such as density, viscosity and thermal conductivity at the interface may lead to numerical difficulties. Therefore, the SPH discrete equations for single phase fluid and phase interface comply with Yang's [17] treatment.

The treatment of phase transition

Droplet mass reduction rate is equal to the liquid evaporation rate. Equation (10), discrete form of eq. (9), is the mass transfer equation for gas particles at the phase interface, and the mass transfer equation for liquid particles is taken as negative for eq. (10) [17]. The evaporative mass transfer process satisfies the mass conservation law. When the droplet particle mass/initial mass is less than 0.5, the droplet particles are merged by particle merging technique and the droplet particle number is reduced to achieve the same phase transition effect as the droplet particles transition from liquid phase to gas phase properties. Equation (11) is the gas phase particle volume mass flux:

$$\dot{m} = \frac{V\nabla(\rho D\nabla Y)}{1-Y} = \frac{m}{(1-Y)}\frac{\mathrm{d}Y}{\mathrm{d}t} \tag{9}$$

$$\dot{m}_{g\ell} = \frac{m_g}{1-Y_g}\frac{2m_\ell D_g(r_g - r_\ell)\nabla_g W_{g\ell}}{\rho_\ell r_{g\ell}^2}(Y_g - Y_\ell) \tag{10}$$

$$\dot{m}'''_{g\ell} = \frac{\dot{m}_{g\ell}}{V_g} = \frac{\rho_g}{1-Y_g}\frac{2m_\ell D_g(r_g - r_\ell)\cdot\nabla_g W_{g\ell}}{\rho_\ell r_{g\ell}^2}(Y_g - Y_\ell) \tag{11}$$

where subscripts g and ℓ are the stand for the gas particle and the liquid particle, respectively.

Algorithm correction

The mass transfer equations of gas

Particle splitting and merging techniques have satisfying results in dealing with large mass difference problems, but there will be too many particles in the region due to the high speed of gas phase particle splitting, resulting in mediocre computational efficiency and particle overlap problems. In this paper, Fick's law is combined to treat water vapor with different components as different gases, and mass transfer eq. (12) is proposed based on eq. (9) to characterize the mass diffusion phenomenon and solve the problem of large density difference of gas phase:

$$\dot{m}_i = \sum_j \frac{m_i}{1-Y_i}\frac{m_j(\rho_i D_i + \rho_j D_j)(r_i - r_j)\cdot\nabla_i W_{ij}}{\rho_i\rho_j r_{ij}^2}(Y_i - Y_j) \tag{12}$$

Particle splitting and merging techniques

In order to solve the problem of large mass difference in the liquid phase, this paper has adopted the particle splitting and merging techniques proposed by Yang and Kong [17] and made certain modifications. The merging process is accompanied by particle splitting to ensure that the number of particles remains unchanged. The process is described as: First, take a reference mass $m_r = \rho_r V^{[2]}$, where ρ_r is the reference density and $V^{[2]}$ is the volume of the particle in two dimensions which is equal to the square of the spacing between the particles. Then, calculate $\gamma = m_a/m_r$ to get the current particle mass ratio γ. When $\gamma < 0.5$, the particle merges into its nearest neighbor. In the left picture of fig. 1, particle a and its nearest neighbor b merge into a new particle located at the center of mass of the two particles. The merging process satisfies conservation of mass, momentum, and energy. Finally, after merging, the gas particles are sorted by mass ratio γ, and the gas particles are split in order of mass ratio from large to small (split number = fusion number). In the right picture of fig. 1, particle a splits into two particles located on a line perpendicular to the line connecting particle a and its nearest particle b, and the distance is taken as $(V^{[2]})^{1/2}/2$.

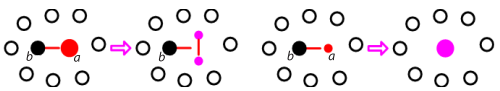

Figure 1. Process of particle splitting and merging

Surface tension

This paper has adopted the surface tension model with large density difference proposed by Yan to prevent particles at the gas-liquid interface from penetrating each other [21]:

$$\overline{c}_i = \sum_{j=1}^{N}\frac{m_j}{\rho_j}c_j W_{ij} \tag{13}$$

$$n_i = \sum_{j=1}^{N} \frac{m_j}{\rho_j}\left(\overline{c}_j - \overline{c}_i\right)\nabla_i W_{ij},\ \ \delta_i = \begin{cases} \dfrac{n_i}{|n_i|}, |n_i| > \xi \\ 0, \text{ else} \end{cases} \tag{14}$$

$$k_i = -\sum_{j=1}^{N} \frac{m_j}{\rho_j}(\delta_j - \delta_i)\nabla_i W_{ij} \tag{15}$$

$$f_s = -\frac{2\sigma}{\rho_i + \rho_j}(\nabla\delta_i)n_i \tag{16}$$

where c_j is the color function, n_i – the normal vector, k_i – the curvature, and δ – the viscosity coefficient. The threshold parameter method of Morris proposes that ξ is usually taken as $0.01/h$ [22]. In view of the large difference in gas-liquid density, the smaller air density leads to a smaller calculated normal direction, so the valve parameter ξ is taken as $0.0001/h$.

Artificial stress

Particle splitting and merging techniques will lead to regional stretching instability. To further effectively eliminate this phenomenon, the artificial stress method proposed by Qiang *et al.* [23] for multi-phase flow with large density difference is introduced, where a small repulsive force is applied between two similar particles to avoid them from coming too close or even aggregating:

$$\frac{\mathrm{d}v_i}{\mathrm{d}t} = -\frac{1}{m_i}\sum_j (V_i^2 + V_j^2) f_{ij}^n \tilde{R}_{ij} \nabla_i W_{ij} \tag{17}$$

$$f_{ij} = \frac{W(r_{ij})}{W(\Delta p)} \tag{18}$$

$$\tilde{R}_{ij} = \frac{\rho_i S_j + \rho_j S_i}{\rho_i + \rho_j},\quad S_k = \begin{cases} -\varepsilon_1 P_k, P_k < 0 \\ \varepsilon_2 P_k, P_k > 0 \end{cases} \tag{19}$$

where r_{ij} is the distance between particles i and j, Δp – the initial spacing of particles, and ε_1 and ε_2 are the both taken as 0.3.

Shephard filtering and XSPH

To reduce the fluctuation of density in the process of SPH simulation, Shephard filtering is applied to reinitialize the density field [24]. The summation is performed only for particles in the same phase. The XSPH correction introduced by Monaghan is used to prevent particle penetrations [14], where ε is 0.05:

$$\tilde{\rho}_a = \frac{\sum_b m_b W_{ab}}{\sum_b V_b W_{ab}} \tag{20}$$

$$\hat{u}_a = u_a + \varepsilon \sum_b \frac{2m_b}{\rho_a + \rho_b}(u_b - u_a) W_{ab} \tag{21}$$

Numerical simulation

Numerical examples to verify surface tension

In order to prevent the mutual penetration of gas and liquid phase, the large density difference surface tension model proposed by Yan *et al.* [21] was introduced. Since there is no gas phase environment in the simulation process in this model, the deformation of square droplet and interfusion of droplets in the gas phase environment were simulated to verify the feasibility of the algorithm.

The calculation and model parameters used in this paper are shown in tab. 1. Figure 2(a) shows the initial SPH particle distribution for the natural rounding model of square droplet. The initial square droplet was 0.3 mm. The droplet was located at the center of square computational domain, which was filled with gas. The length of the square was 2.4 mm. The initial particle spacing was 0.04 mm. Figure 3 selects the simulation diagrams of the square droplet at 0.2 ms, 0.6 ms, 1 ms, and 5 ms and compares it with the natural rounding of square droplet under the quintic spline kernel function in fig. 4, and the variation process is closer. Figure 2(b) shows the initial SPH particle distribution for droplet interfusion model. Both droplets had a radius of 0.3 mm. They were located at the center of a square computational domain, which was filled with gas. The length of the square was 2.4 mm. The initial particle spacing was 0.04 mm. Figure 5 selects the simulation diagrams of droplet interfusion at 0.5 ms, 1 ms, 2 ms, and 5 ms, and the two droplets are fused into a good circular droplet after a slight oscillation.

Table 1. Physical properties of the liquid and gas

	ρ [kgm^{-3}]	k [Wm^{-1}K^{-1}]	μ (kgm^{-1}s^{-1})	C_p (Jkg^{-1}K^{-1})	h_v (Jkg^{-1})	D_v (m^{2}s^{-1})	T [K]
Liquid	1000	0.6	0.001	4180	2300000	–	353
Gas	1.2	0.046	0.00002	1000	–	0.00002	373

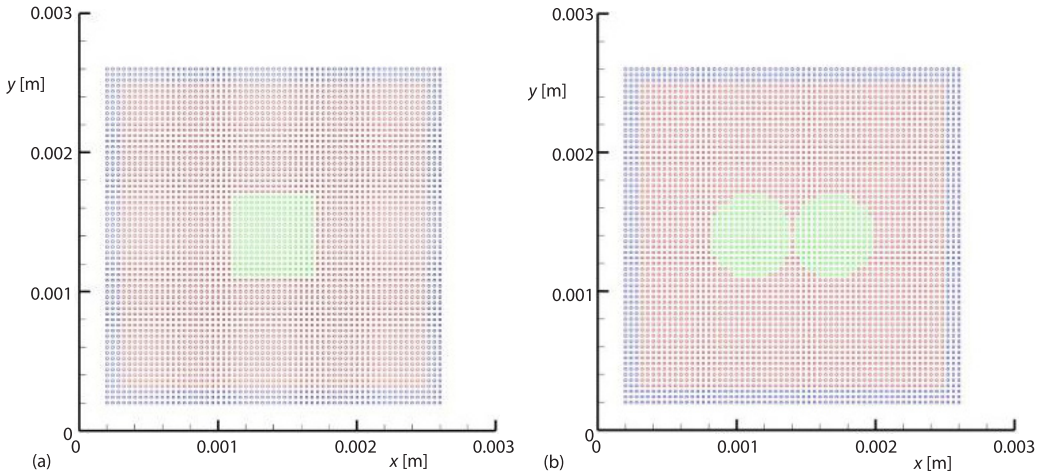

Figure 2. (a) Natural rounding model of square droplet and (b) model of single droplet evaporation without gravity

Numerical simulation

Figure 6(a) shows the initial SPH particle distribution for model of single droplet evaporation without gravity. The initial radius of the droplet was 0.3 mm. The droplet was located at

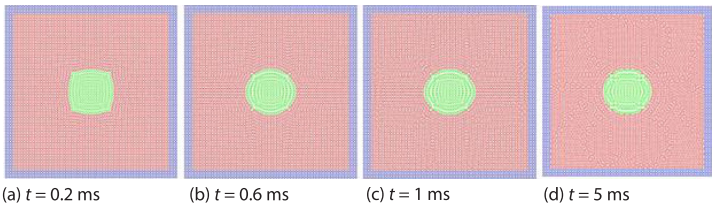

Figure 3. Variation process of square droplet based on hyperbolic kernel function

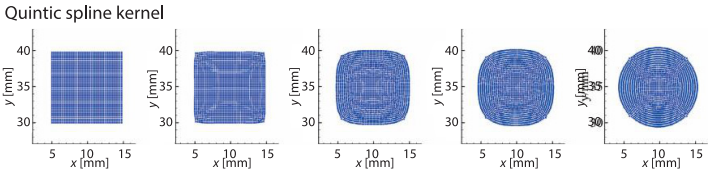

Figure 4. Variation process of square droplet based on quintic spline kernel function

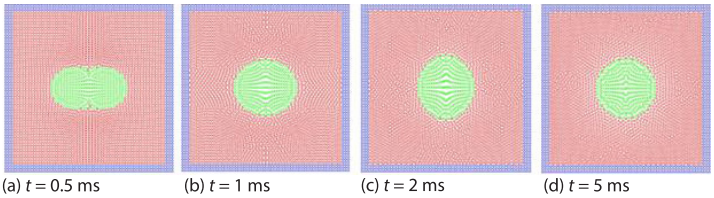

Figure 5. Variation process of droplet interfusion

the center of a square computational domain, which was filled with gas. The length of the square was 2.4 mm. The initial particle spacing was 0.04 mm. Figure 6(b) shows the initial SPH particle distribution for model of interacting droplet evaporation without gravity. The initial radius of droplets was 0.2 mm. To avoid the influence of the boundary on evaporation, the droplets were always kept 2 mm away from the boundary. The initial particle spacing was 0.04 mm.

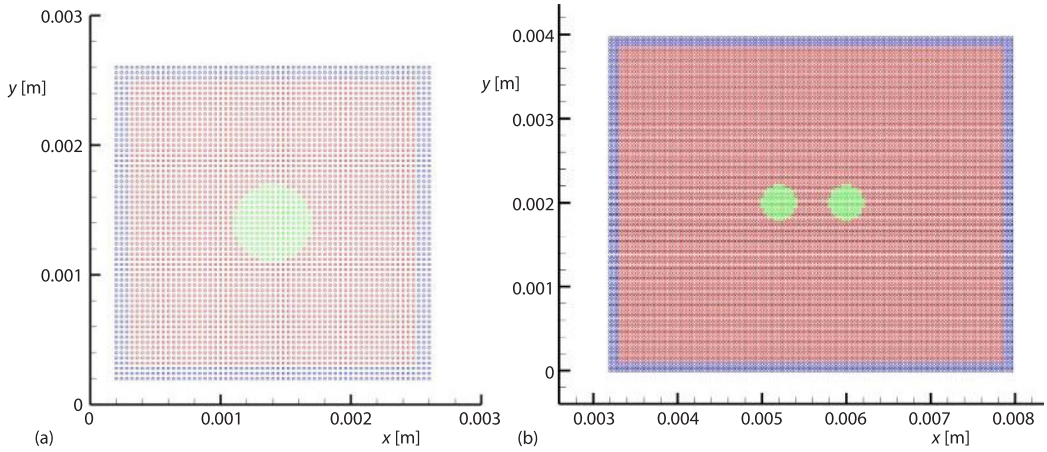

Figure 6. (a) Model of single droplet evaporation without gravity and (b) model of interacting droplet evaporation without gravity

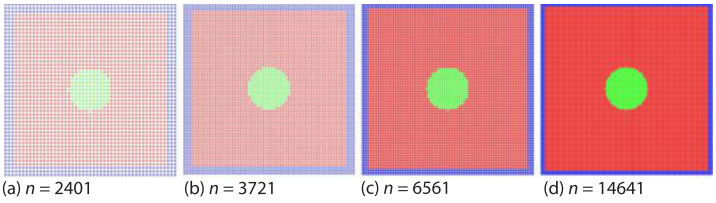

Figure 7. Evaporation models with different particle number

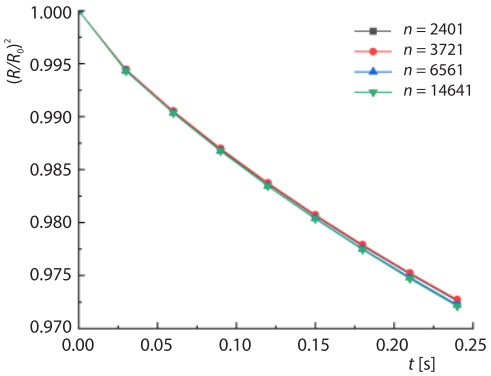

Figure 8. Evaporation curves with different particle number

The number of particles in the model established in this paper was n = 3721. In order to verify that the model presented had no influence on the evaporation process of droplet, models with the number of particles n = 2401, 3721, 6561, and 14641 were selected for simulation as shown in fig. 7. The simulation results are shown in fig. 8. The evaporation curves of the droplet in the figure almost coincide, and the model in this paper has almost no influence on the evaporation process of the droplet.

The evaporation state of 0-3 seconds during the simulation is selected. Figure 9 shows the variation process of single droplet evaporation and the droplet gradually shrinks. Figure 10 displays the variation process of temperature. The droplet temperature gradually decreases with the energy consumption in the evaporation process. The second term of the eq. (5) is the energy required by the droplet phase transition. Part of the energy absorbed from the surrounding environment will lead to a decrease in the gas phase temperature, and part of the energy taken away from the droplet surface by the water molecules during the evaporation process will lead to a gradual decrease in the droplet temperature. Figure 11 presents the variation process of vapor mass fraction Y. The variation of mass fraction Y decreases with temperature, thus the evaporation rate slows down until the evaporation process reaches a steady-state. Fig-

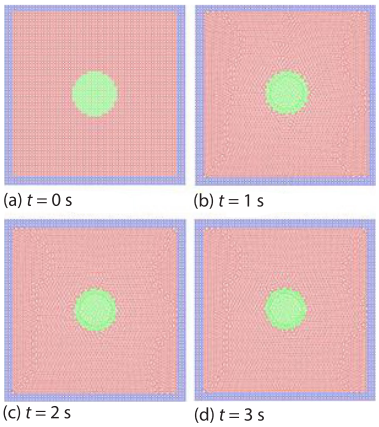

Figure 9. Variation process of single droplet evaporation

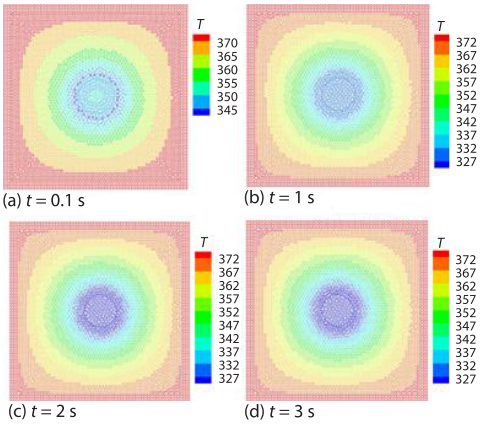

Figure 10. Variation process of temperatured

ure 12 shows the variation process of gas particle mass. In the early evaporation process, the gas particle mass changes rapidly. As the evaporation gradually slows down, the change of gas particle mass gradually flattens out and reaches a stable state.

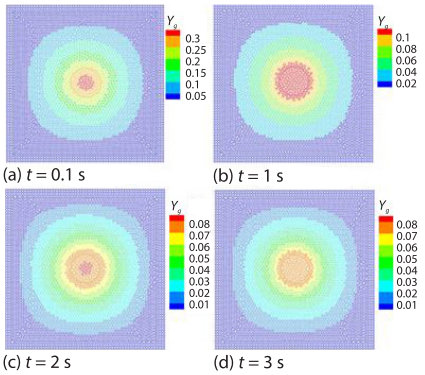

Figure 11. Variation process of vapor mass fraction *Y*

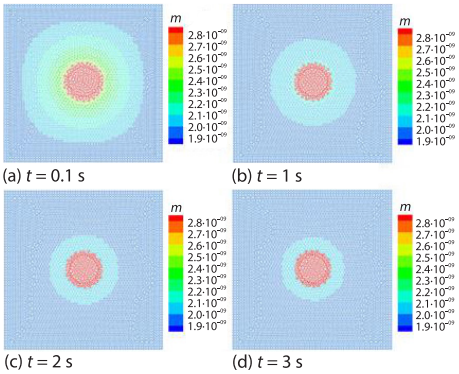

Figure 12. Variation process of gas particle mass

According to [25], the droplet surface temperature is an important parameter for mass diffusing controlled evaporation. The surface temperature used to calculate the evaporation time is a constant value, but the surface temperature is a variable in the evaporation process. Therefore, the maximum and minimum values of droplet surface temperature in the evaporation process are taken to calculate the droplet evaporation time, respectively, and compares with the simulated values. Figure 13 shows the comparison between SPH simulated evaporation time and theoretical evaporation time of upper and lower limit temperatures. In the simulated evaporation process of 2.4 seconds, the maximum surface temperature of the droplet is 353 K, and Y is about 0.3545, then the theoretical evaporation time is 4.2835 seconds. The lowest surface temperature of the droplet is 321 K, and Y is about 0.075, then the theoretical evaporation time is 24.0503 seconds. At the early stage of evaporation, droplet temperature is high and evaporation is more intense, the evaporation time curve of SPH simulation is close to the theoretical evaporation time curve at $Y = 0.3545$ in the figure. As energy is consumed in the evaporation process, the temperature of the droplet decreases and the evaporation rate slows down, and the evaporation time curve of SPH simulation is close to the theoretical evaporation time curve at $Y = 0.075$ in the figure.

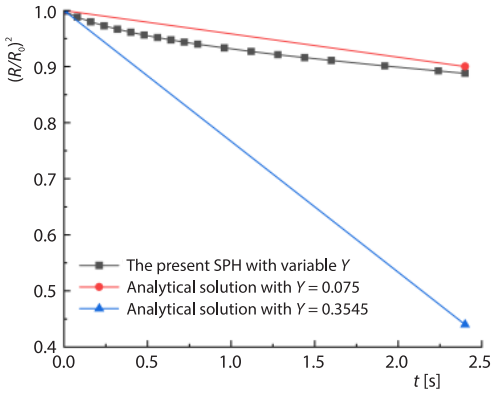

Figure 13. Comparison between SPH simulated evaporation time and theoretical evaporation time of upper and lower limit temperatures

In order to study the influence between interacting droplets in the process of evaporation, interacting droplet evaporation with $C = 2$, 3, 6, 8, 9, 10 and single droplet evaporation with $C = 10$ were set for numerical simulation. Figures 14 and 15 show the variation process of temperature and vapor mass fraction Y for $C = 2$, 7, and 10 interacting droplets and $C = 10$ single droplet for 0.1 second evaporation, respectively. In these figures, the effect of temperature field and vapor mass fraction between droplets decreases as C increases.

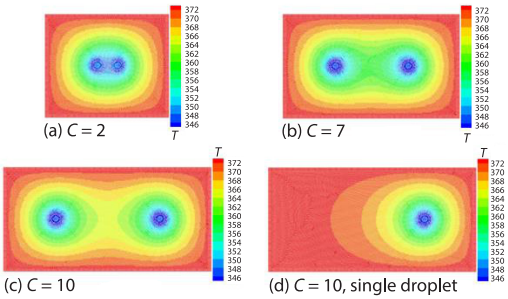

Figure 14. Variation process of temperature for C = 2, 7, and 10 interacting droplets and C = 10 single droplet

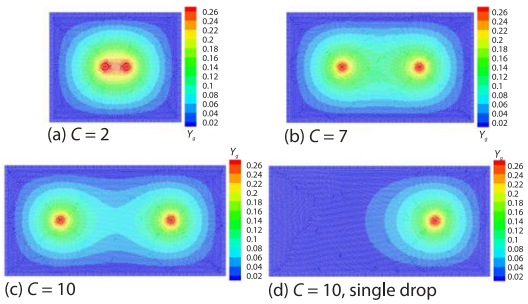

Figure 15. Variation process of vapor mass fraction Y for C = 2, 7, and 10 interacting droplets and C = 10 single droplet

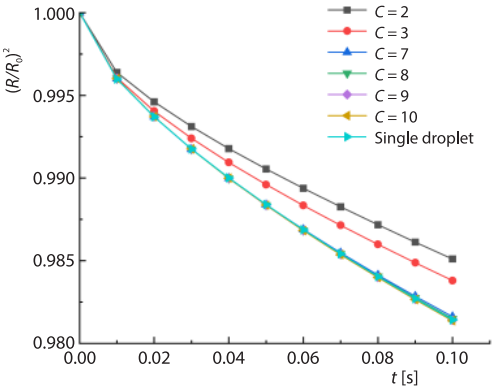

Figure 16. Comparison of evaporation time between C = 2, 3, 6, 8, 9, and 10 interacting droplets and C = 10 single droplet

Figure 16 shows the comparison of evaporation time between C = 2, 3, 6, 8, 9, and 10 interacting droplets and C = 10 single droplet. In the simulated evaporation process of 0.1 second, the evaporation time curves of interacting droplets with C = 9 and 10 are almost approximately the same as those of single droplet. So when $C > 8$, the influence between the interacting droplet evaporation can be ignored.

Conclusions

Based on the integrated SPH method, the following conclusions are obtained by simulating the non-gravity single droplet evaporation and interacting droplet evaporation, are as follows.

- Based on the SPH numerical model, the evaporation time of single droplet is simulated. The evaporation time conforms to D^2 *law* and is compared with the theoretical evaporation time, which is within the allowable range of the theoretical evaporation time.
- The influence between interacting droplets is very important in the process of evaporation. The numerical simulation based on the model in this paper shows that the influence can be ignored only when $C > 8$.
- In the simulation of the aforementioned two evaporation examples, the mass transfer equation and particle splitting and merging techniques can better solve the problem of mass difference at the phase interface, mass transfer equation can better characterize the mass diffusion phenomenon of the gas phase, and the particle number remains unchanged. No penetration phenomenon of particles of different phases appears at the phase interface. This shows that the numerical model of multi-phase heat and mass transfer based on the gas phase SPH mass transfer equation proposed can be used to simulate and analyze phase transition problems with large density difference.

Acknowledgment

This work is supported by National Natural Science Foundation of China (12002296), Xinjiang Uygur Autonomous Region Key Research and Development Task Special Project

(2022B03028-5), Major Science and Technology Special Project of Xinjiang Uygur Autonomous Region (2022A01002-2), Xinjiang Uygur Autonomous Region Youth Talent Support Project (2022TSYCCX0054).

Nomenclature

C – droplet spacing/ droplet diameter, [–]
C_p – specific heat capacity, [Jkg^{-1}K^{-1}]
D – mass diffusivity, [m2s^{-1}]
c – numerical speed of sound, [–]
h – smoothing lenth, [m]
h_v – latent heat, [Jkg^{-1}]
k – thermal conductivity, [Wm^{-1}K^{-1}]
m – mass, [kg]
$\dot{m}$ – mass evaporation rate, [kgm^{-2}s^{-1}]
$\dot{m}'''$ – volumetric mass evaporation rate, [kgm^{-5}s^{-1}]
p – pressure, [Pa]
r – distance between particles, [m]
T – temperature, [K]
u – velocity, [ms^{-1}]
V – volume, [m^3]
Y – vapor mass fraction, [–]

Greek symbols

δ – surface tension coefficient, [Nm^{-1}]
μ – dynamic viscosity
ρ – density, [kgm^{-3}]

References

[1] Godsave, G. A. E., Studies of the Combustion of Drops in A Fuel Spray – The Burning of Single Drops of Fuel, *Symposium (International) on Combustion*, *4* (1953), 1, pp. 818-830
[2] Spalding, D. B., The Combustion of Liquid Fuels, *Symposium (International) on Combustion*, *4* (1953), 1, pp. 847-864
[3] Nomura, H., *et al*., Experimental Study on High-Pressure Droplet Evaporation Using Microgravity Conditions, *Symposium (International) on Combustion*, *26* (1996), 1, pp. 1267-1273
[4] Labowsky, M., Calculation of the Burning Rates of Interacting Fuel Droplets, *Combustion Science and Technology*, *22* (1980), 5-6, pp. 217-226
[5] Sangiovanni, J. J., Labowsky M., Burning Times of Linear Fuel Droplet Arrays: A Comparison of Experiment and Theory, *Combustion and Flam*e, *47* (1982), 0010-2180, pp. 15-30
[6] Marberry, M., *et al*., Effect of Multiple Particle Interactions on Burning Droplets, *Combustion and Flame*, *57* (1984), 3, pp. 237-245
[7] Castanet, G., *et al*., Evaporation of Closely-Spaced Interacting Droplets Arranged in a Single Row, *International Journal of Heat and Mass Transfer*, *93* (2016), 0017-9310, pp. 788-802
[8] Chiang, C. H., Sirignano, W. A., Interacting, Convecting, Vaporizing Fuel Droplets with Variable Properties, *International Journal of Heat and Mass Transfer*, *36* (1993), 4, pp. 875-886
[9] Tanguy, S., *et al*., A Level Set Method for Vaporizing Two-Phase Flows, *Journal of Computational Physics*, *221* (2007), 2, pp. 837-853
[10] Safari, H., *et al*., Consistent Simulation of Droplet Evaporation Based on the Phase-Field Multi-Phase Lattice Boltzmann Method, *Physical Review E*, *90* (2014), 3, 033305
[11] Safari, H., *et al.*, Extended Lattice Boltzmann Method for Numerical Simulation of Thermal Phase Change in Two-Phase Fluid-Flow, *Physical Review E*, *88* (2013), 1, 013304
[12] Nikolopoulos, N., *et al*., A Numerical Investigation of the Evaporation Process of a Liquid Droplet Impinging on a Hot Substrate, *International Journal of Heat and Mass Transfer*, *50* (2007), 1-2, pp. 303-319
[13] Tonini, S., Cossali, G. E., A Multi-Component Drop Evaporation Model Based on Analytical Solution of Stefan-Maxwell Equations, *International Journal of Heat and Mass Transfer*, *92* (2016), 0017-9310, pp. 184-189
[14] Monaghan, J. J., Smoothed Particle Hydrodynamics, *Annual Reviews of Astronomy and Astrophysics*, *30* (1992), pp. 543-574
[15] Monaghan, J. J., *et al.*, Solidification Using Smoothed Particle Hydrodynamics, *Journal of Computational Physics*, *206* (2005), 2, pp. 684-705
[16] Zhang, B. W., *et al*., Numerical Simulation of Droplet Impinging Icing Process on a Low Temperature Wall with Smoothed Particle Hydrodynamics Method, *Thermal Science*, *26* (2022), 4B, pp. 3373-3385
[17] Yang, X. F., Kong, S. C., Smoothed Particle Hydrodynamics Method for Evaporating Multi-Phase Flows, *Physical Review E*., *96* (2017), 3, 033309
[18] Wang, D. D., *et al*., Numerical Simulation of Droplet Evaporation Based on Smooth Particle Fluid Dynamics Method (in Chinese), *Journal Of Propulsion Technology*, *42* (2021), 02, pp. 382-394

[19] Li, L. H., *et al*., The SPH-ASR Study of Drop Impact on a Heated Surface with Consideration of Inclined Angle and Evaporation, *Engineering Analysis with Boundary Elements*, *141* (2022), 0955-7997, pp. 235-249
[20] Cleary, P. W., Modelling Confined Multi-Material Heat and Mass-Flows Using SPH, *Applied Mathematical Modelling*, *22* (1998), 12, pp. 981-993
[21] Yan S. L., *et al*., Study on the Flow and Heat Transfer of Water Droplets Hitting a Constant Temperature Wall Based on Sph Method (in Chinese), *Energy Engineering*, *01* (2018), pp. 1-8
[22] Morris, J. P., Simulating Surface Tension with Smoothed Particle Hydrodynamics, *International Journal for Numerical Methods in Fluids*, *33* (2000), 3, pp. 333-353
[23] Qiang, H. F., *et al*., Numerical Simulation of 2-D Droplet Vollision Based on SPH Method of Multi-Phase Flow with Large Density Difference (in Chinese), *Acta Physica Sinica*, *62* (2013), 21, 214701
[24] Bonet, J., Lok, T. S. L., Variational and Momentum Preservation Aspects of Smooth Particle Hydrodynamic Formulations, *Computer Methods in Applied Mechanics and Engineering*, *180* (1999), 1-2, pp. 97-115
[25] Turns, S. R., *Introduction Combustion*, McGraw-Hill Companies, New York, USA, 1996

Paper submitted: March 11, 2023
Paper revised: April 21, 2023
Paper accepted: April 22, 2023